RSC Advances

PAPER

View Article Online
View Journal | View Issue

Cite this: *RSC Adv.*, 2021, **11**, 7231

Influence of low Bi contents on phase transformation properties of VO_2 studied in a VO_2:Bi thin film library†

Xiao Wang, [a] Detlef Rogalla,[b] Aleksander Kostka[c] and Alfred Ludwig *[ac]

A thin-film materials library in the system V–Bi–O was fabricated by reactive co-sputtering. The composition of Bi relative to V was determined by Rutherford backscattering spectroscopy, ranging from 0.06 to 0.84 at% along the library. The VO_2 phase M1 was detected by X-ray diffraction over the whole library, however a second phase was observed in the microstructure of films with Bi contents > 0.29 at%. The second phase was determined by electron diffraction to be $BiVO_4$, which suggests that the solubility limit of Bi in VO_2 is only ~0.29 at%. For Bi contents from 0.08 to 0.29 at%, the phase transformation temperatures of VO_2:Bi increase from 74.7 to 76.4 °C by 8 K per at% Bi. With X-ray photoemission spectroscopy, the oxidation state of Bi was determined to be 3+. The V^{5+}/V^{4+} ratio increases with increasing Bi content from 0.10 to 0.84 at%. The similarly increasing tendency of the V^{5+}/V^{4+} ratio and T_c with Bi content suggests that although the ionic radius of Bi^{3+} is much larger than that of V^{4+}, the charge doping effect and the resulting V^{5+} are more prominent in regulating the phase transformation behavior of Bi-doped VO_2.

Received 13th November 2020
Accepted 4th February 2021

DOI: 10.1039/d0ra09654g

rsc.li/rsc-advances

1. Introduction

The correlated electron material VO_2 has been widely researched due to its metal to insulator transition (MIT), which takes place at a critical temperature (T_c) of ~68 °C.[1–3] The MIT of VO_2 is accompanied by a structural phase transformation from the monoclinic structure at $T < T_c$ to the tetragonal structure at $T > T_c$. Across the MIT, the electrical resistivity of VO_2 changes up to 5 orders of magnitude and the optical transmittance in the infrared spectral region changes from highly transparent to reflective. These properties make it promising for applications such as smart windows,[4,5] Mott-transition FET[6] and nano-actuators.[7,8]

For practical use, the T_c of VO_2 needs to be tailorable to fulfill the different demands of applications. Among the approaches of tuning T_c, an addition of a third element (frequently called elemental doping) has been widely studied. Furthermore, by investigating the influence of additional elements on the MIT properties of VO_2, more insights into the mechanism of the MIT can be gained.[9–11] The debate over the MIT mechanism has lasted for decades, with two perspectives, either attributing the MIT to electron correlation (Mott-transition) or lattice structure change (Peierls-transition).[12–15]

Most dopants can be categorized into two groups: (I) includes those with higher ionic radii and valence compared to V^{4+}, *e.g.*, W^{6+}, Mo^{6+}, Nb^{5+};[16–18] (II) includes those with smaller ionic radii and lower valence, *e.g.*, Cr^{3+}, Al^{3+}.[19,20] Addition of group I elements to VO_2 reduces T_c values, which is sometimes ascribed to the lattice distortion induced by the dopant, while others attribute the reduced T_c to the charge doping and increased carrier density stemming from the dopants.[10,21,22] Concerning group II, additional phases of VO_2 can form as a result of doping, *e.g.*, M2 and T phase, making these systems more complex. In summary, it is still not well determined whether the change of T_c is due to a structural change or a charge effect. Recently, research on rare-earth doped VO_2 provides more insights, as those elements have higher ionic radii but lower valence than V^{4+}.[23] *E.g.*, Eu^{3+} was reported to decrease T_c by 6.5 K per at%; Tb^{3+} leads to a reduction of T_c at lower level of element content (<5 at%) and an increment at higher levels.[23,24]

In this work, Bi is chosen as dopant, because Bi^{3+} has a 78% higher ionic radius (0.103 nm) but lower valence compared to V^{4+}. The crystalline structure, composition, microstructure and phase transformation properties of Bi-doped VO_2 in form of a thin film composition spread are studied to get more insights into the effect of this dopant on the MIT of VO_2.

2. Experimental

The thin film samples were fabricated by reactive co-sputtering on a 100 mm long, 5 mm wide Si (100) strip from a V target

[a]*Chair for Materials Discovery and Interfaces, Institute for Materials, Faculty of Mechanical Engineering, Ruhr-Universität Bochum, D-44801 Bochum, Germany*
[b]*RUBION, Ruhr-Universität Bochum, D-44801 Bochum, Germany*
[c]*Zentrum für Grenzflächendominierte Höchstleistungswerkstoffe (ZGH), Ruhr-Universität Bochum, D-44801 Bochum, Germany. E-mail: alfred.ludwig@rub.de*

† Electronic supplementary information (ESI) available. See DOI: 10.1039/d0ra09654g

(99.95% purity, 100 mm diameter, Nova Fabrica) and a Bi_2O_3 target (99.9% purity, 100 mm diameter, Evochem) using a magnetron sputter system (AJA International, USA). Fig. 1 shows the geometric layout of the two targets and the substrate. V and Bi_2O_3 targets are positioned opposite to each other, and the Si strip is positioned along the V–Bi_2O_3 target direction. During the deposition, the substrate was static. As a result, the amount of sputtered material on the substrate strip varies at different positions with regard to the relative distance between the target and substrate. Empirically, the spatial profile of thickness in the used setup follows roughly a linear decrease along the library (from substrate positions closer to the source to positions further apart from the source), which is illustrated by the wedge shape of the thickness distribution of deposited material for each source in Fig. 1. Due to the spatial profile of the sputtered V and Bi atoms, a continuous Bi gradient forms along the strip, which is hereinafter referred to as VO_2:Bi library. Pulsed DC power of 300 W (pulsing frequency of 10 kHz, reverse time of 5 μs) was applied to the V target and rf power of 10 W was applied to Bi_2O_3. For sputtering, 80 sccm of Ar was introduced into the chamber and the process pressure was set to 0.4 Pa. A plasma emission monitor (PEM) system (Flotron, Nova Fabrica, Lithuania) was used to dynamically control the oxygen flow rate, in order to obtain single phase VO_2. Details about the control mechanism can be found elsewhere.[25] The oxygen flow was about 6.4 sccm. The deposition temperature was 520 °C.

For the characterizations, measurement areas (MAs) were defined every 9 mm along the strip (Fig. 1). The crystalline structure of the library was determined by X-ray diffractometry (XRD, Bruker D8 Discover). The composition spread of the library was studied using Rutherford backscattering spectrometry (RBS) at the 4 MV accelerator facility of RUBION/Ruhr University Bochum, with a measurement spot size of 1 mm. Oxidation states of V and Bi were investigated by X-ray photoelectron spectroscopy (XPS, Kratos Axis Nova) using Al Kα as exciting source. Microstructure and morphology of the library was studied by scanning electron microscope (SEM, Jeol JSM-7200F). Transmission electron microscopy (TEM, Jeol JEM-2100Plus) was performed on selected areas using cross-sectional samples. The phase transformation properties of the library were studied by temperature-dependent resistivity $\rho(T)$ measurements using four-probe method. A four-point probe head with 20 pins (5 × 4 groups) was used, which can measure five MAs simultaneously to achieve high throughput. The distance between the pins is 0.5 mm and the distance between each group of pins is 4.5 mm. During the measurement, the library is fixed on a temperature-controlled stage, with temperature cycling from 20 °C to 100 °C and temperature stability of ± 0.05 °C.

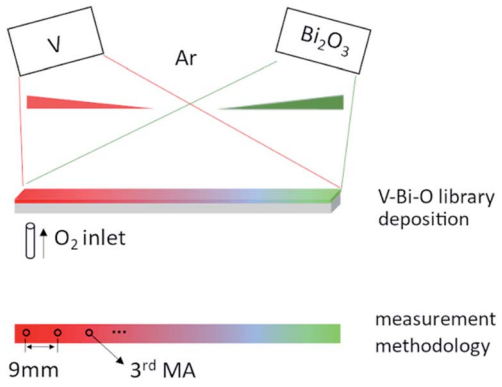

Fig. 1 Schematic (not to scale) of the co-sputter deposition of the VO_2:Bi library and its measurement areas (MAs) for characterizations (top view), the wedge shapes in the schematic denote the thickness gradients of sputtered material from each target in the library.

3. Results and discussion

3.1 Composition spread and crystalline structure

Fig. 2a shows RBS spectra of the VO_2:Bi library with well-separated and background-free bands for V and Bi. All spectra are well simulated with SIMNRA software and areal densities for V and Bi were determined, from which the relative Bi content was calculated as shown in Fig. 2b.[26] The Bi content increases from about 0.06 at% at the V-rich side to 0.84 at% at the Bi-rich side of the library. It is noteworthy that the Bi content here is the ratio Bi/(V + Bi), not the Bi proportion of the whole thin film composition. The absolute values of the areal densities for Bi and V determined by RBS have experimental errors of about 8% due to a systematic uncertainty in the normalization of the detection setup. The Bi/(Bi + V) ratio, however, is independent from the normalization, because it is cancelled out. The residual uncertainty is given by the statistical

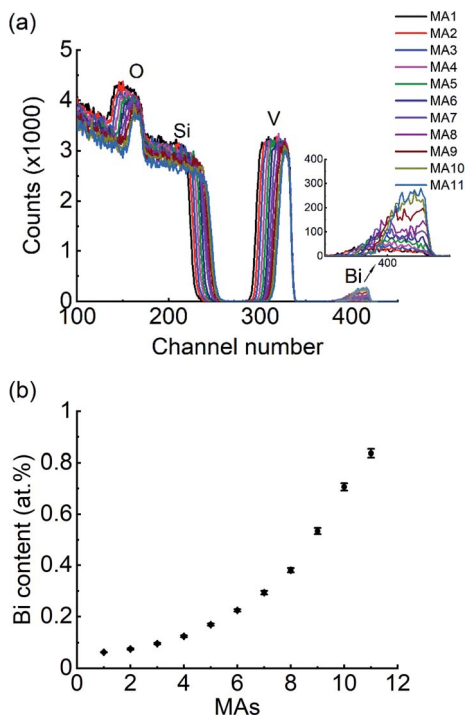

Fig. 2 (a) RBS spectra acquired from all MAs of the V–Bi–O library. The inset is an enlarged Bi channel. (b) Bi content (Bi/(Bi + V) ratio) along the library with error marked, which is within 4% (relative error).

errors of the element signals. Even though there is only a very little amount of Bi, the RBS signal can be well analyzed and has a statistical error of 3% (about 1% for the V signal). The resulting relative error of the ratio is almost 4%, *e.g.*, 0.84 ± 0.03 at% for MA11.

The RBS spectra also give information about the thickness variation along the library. Film thicknesses could be determined non-destructively by a calculation based on measured areal density and density of VO_2. Since there is no referable density data of $V_{1-x}Bi_xO_2$ films, the density of VO_2 (4.67 g cm^{-3}) was used. This estimate is acceptable due to the low Bi content in the library. Based on the calculation, the thickness of film ranges from 206 nm at the V-rich end (1st MA) to 77 nm at the Bi-rich end (11th MA), which also shows a tendency of linear decease as presented in the ESI (Fig. S1).†

Fig. 3 shows the XRD patterns from V-rich to Bi-rich sides of the VO_2:Bi library. All films show almost identical diffractions patterns. The diffraction peaks appear at 2θ = ~27.9°, 37.1°, 39.8°, 55.6°, 57.8°, which can be indexed as (011), (21−1), (002), (220), (022) of VO_2 M1 respectively. Unlike Cr- and Al-doped VO_2, no M2 or T phases were observed in VO_2:Bi library, probably due to the low amount of Bi. Similarly, no bismuth oxides were detected by XRD neither. A detailed analysis on the (011) peaks are presented in the ESI (Fig. S2).† The main (011) peaks in all XRD patterns in Fig. 3 did not show obvious position shift with increase of Bi, and the overall (011) peak position of the VO_2:Bi thin film is about 27.98° ± 0.02°. Only a decrease in the peak intensity was observed, which might be attributed to decreased film thicknesses in the library.

3.2 Analysis of the oxidation states by XPS spectroscopy

Fig. 4a shows the V2p–O1s XPS spectrum of a 0.17 at% Bi–VO_2 sample with peak fitting illustrated. Spectra from other MAs are similar with respect to peak position and peak shape (Fig. 4c). Details about peak fitting can be found elsewhere.[27] The V2p$_{3/2}$ peak in Fig. 4a is asymmetric with a shoulder towards the higher binding energy, which indicates the existence of V^{5+} component in the spectrum, although no other V_2O_{2n+1} phase was observed in the XRD patterns. In deconvolution of V2p$_{3/2}$ peak, two components appear at 516.1 and 517.3 eV, corresponding to V^{4+} and V^{5+} respectively. Given that the detection depth of XPS is generally well below 10 nm, the V^{5+} signal might be partly ascribed to surface oxidation of VO_2. By using the same fitting parameters, deconvolution was performed on all spectra of the library using the software ESCApe (Kratos) and the V^{5+}/V^{4+} ratio was plotted against the Bi content in Fig. 4b with quantification error indicated. At the V-rich side of the library (MA1, MA2), the amount of V^{5+} is higher and drops. From 3rd MA on, the V^{5+}/V^{4+} ratio increases with Bi content along the library. Fig. 4a inset shows the Bi 4f spectrum from the 0.17 at% Bi–VO_2 sample. The Bi 4f$_{7/2}$ appears at ~159.4 eV, indicating a valence of +3. XPS spectra of Bi from different MAs are also quite similar with respect to the peak position and shape, but with different peak intensity due to different Bi contents.

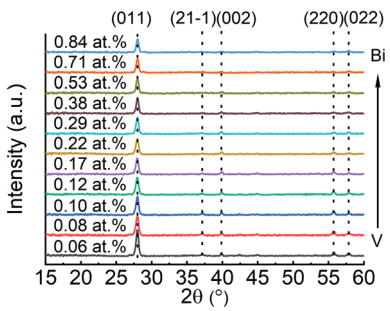

Fig. 3 Stacked XRD patterns of the VO_2:Bi library at different MAs.

3.3 Analysis of microstructure by electron microscopy

The microstructures of the films in the VO_2:Bi library are displayed in Fig. 5. The films of Bi ranging from 0.06 to 0.17 at% exhibit similar dense morphology with grain size in the range of ~100–200 nm, and the grains show sharp facets. For the Bi of 0.22 and 0.29 at%, the grains' facets tend to be blunt, and some grains grow up to size of ~270 nm. From Bi content of 0.38 at%, there is another feature appearing on the surface with bright contrast, as shown in Fig. 5. It seems to emerge at the grain boundary area of VO_2. With increasing Bi content to 0.84 at%, the appearance of the feature does not change significantly, instead its surface coverage largely increases.

A TEM cross-sectional sample with the feature included was prepared using focused ion beam (FIB) to further study this area. Fig. 6b shows the cross-sectional HAADF image of the 0.38 at% Bi–VO_2 film. As the contrast of the image is associated with the atomic number Z, the brighter structures visible at the bottom and the top of the film indicate the presence of a second phase consisting of heavier elements compared to VO_2. A corresponding EDX map shown in Fig. 6c reveals that the second phase contains Bi. Fig. 6d show a bright field image where the Bi-rich grains are in the Bragg contrast. An acquired selected area diffraction (SAD) pattern from this region (Fig. 6e) allows to identify the diffraction spot belonging to the Bi-rich phase, marked as DF. The measured interplanar distance of 0.314 nm corresponds to the (112) plane of the $BiVO_4$ phase – well visible in the dark-field image in Fig. 6f. Fig. 6g and h show the VO_2 phase in the Bragg contrast and its indexed SAD pattern.

Although no $BiVO_4$ was detected by XRD in the library, the detailed microstructure study reveals that the solubility limit of Bi into VO_2 is about ~0.29 at%. Compared to the reported content of other dopants, *e.g.*, 2.5 at% of W, the solubility of Bi into VO_2 is much lower, which might be attributed to the large difference in the ionic radius (0.103 nm for Bi^{3+} *versus* 0.058 nm for V^{4+}). In addition, it is interesting to observe in the TEM image that the $BiVO_4$ does not form a columnar structure as VO_2 does. Instead, the phase is discontinuously formed at the grain boundary of VO_2 on the top of the surface and at the VO_2 film–substrate interface.

3.4 Analysis of phase transformation properties by temperature-dependent resistivity measurements

The phase transformation properties of the library were studied by temperature-dependent resistance measurements ($R(T)$). The

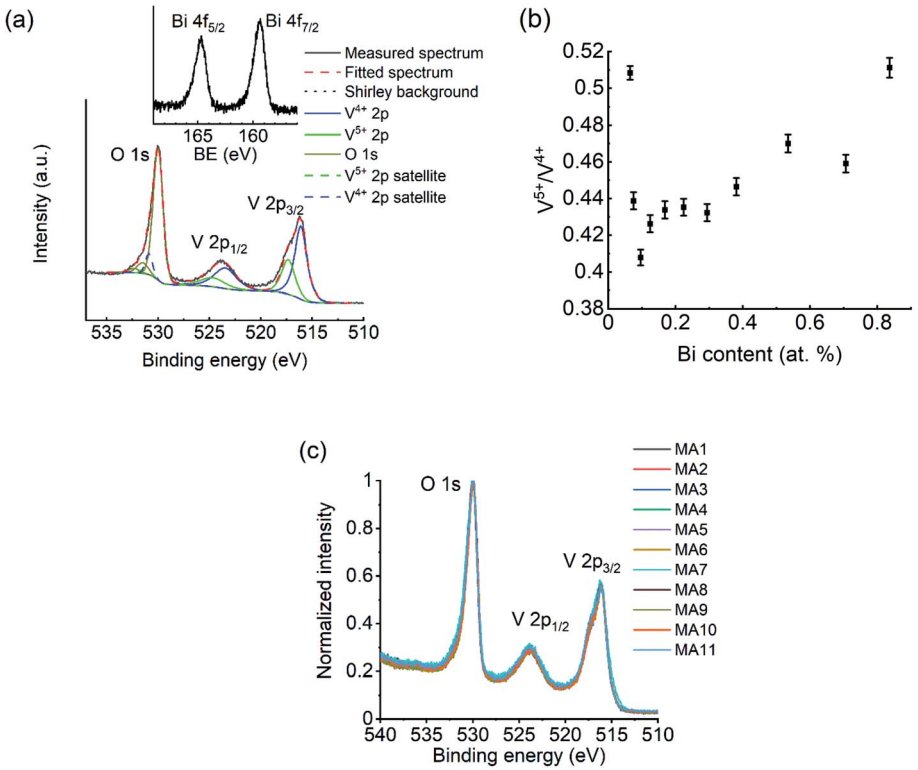

Fig. 4 (a) XPS spectrum of a VO_2:Bi sample with 0.17 at% Bi content. The V2p–O1s region is shown and deconvoluted to its components. The inset shows the spectrum of Bi 4f. (b) The V^{5+}/V^{4+} ratio from the deconvolution is shown in dependence of Bi content, with quantification error indicated. (c) V2p–O1s spectra from different MAs.

temperature-dependent resistivity $\rho(T)$ of the thin film was calculated using film thickness t: $\rho = 4.532 \times t \times R$. Fig. 7a shows $\rho(T)$ curves of the library: the films show resistivity drops of about 3 orders of magnitude across the MIT. With increasing Bi content, the resistivity drop decreases to above 2 orders of magnitude as the resistance of the metallic state increases. Meanwhile, the hysteresis loops of $\rho(T)$ curves become slightly wider. T_c were determined by the first derivative of the heating $\rho(T)$ curve, d log ρ/dT, which was plotted as a function of Bi content in Fig. 7b. The T_c at the V-rich side is 75.2 °C and decreases to 74.7 °C for the 0.08 at% Bi–VO_2 film. Within the Bi content range from 0.08 to 0.29 at%, T_c increases by ~2 K from 74.7 to 76.4 °C. For higher Bi contents of 0.38–0.84 at%, there is only a slight change of ~0.4 K. A partial linear fit was performed in the T_c-increasing section (0.08–0.29 at%) and it was determined that the T_c increases by 8 K per at% Bi. The slight change in T_c for Bi > 0.29 at% is in good agreement with the discovery in microstructure observation, *i.e.*, the second phase $BiVO_4$ is

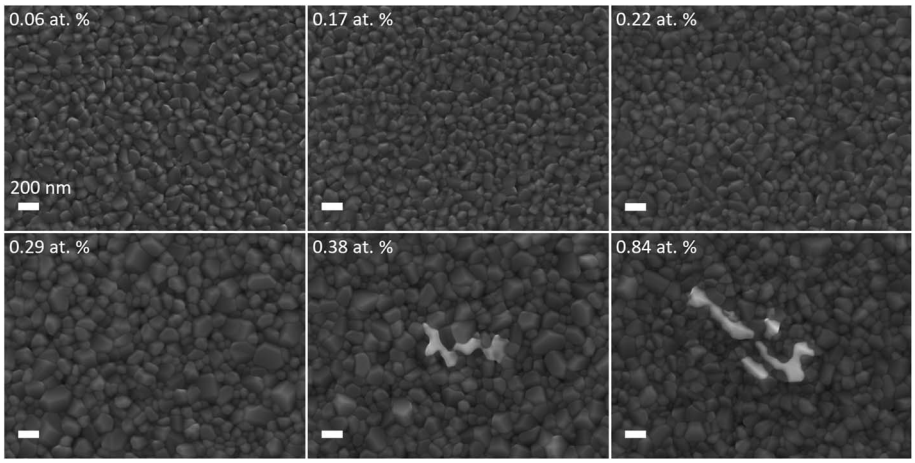

Fig. 5 SEM surface images of films from the VO_2:Bi library with different Bi contents.

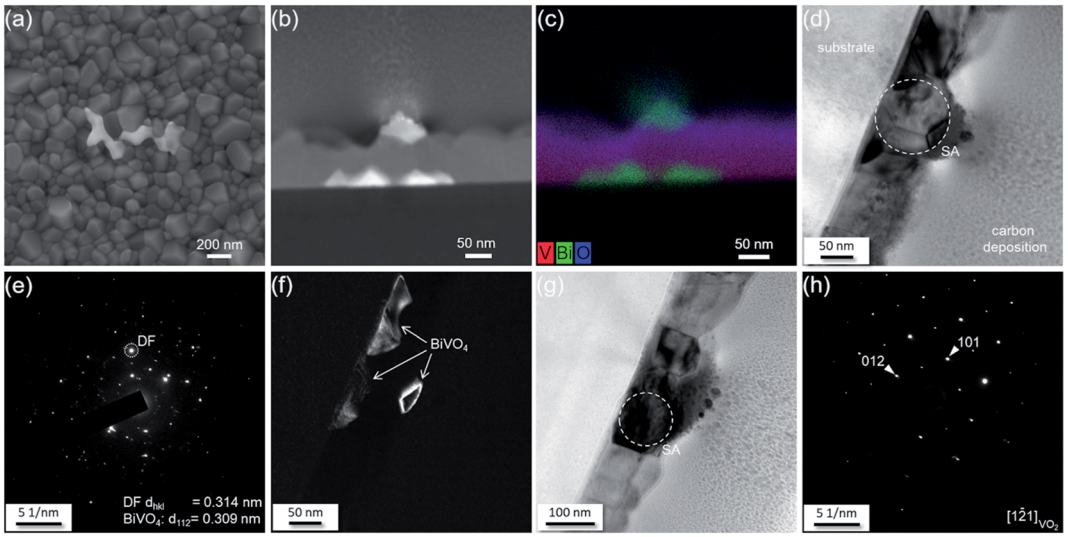

Fig. 6 Results of electron microscopy characterizations. (a) SEM image showing a second phase on the surface of the 0.38 at% Bi–VO_2 film. (b) HAADF image of the film with (c) corresponding EDX map. (d) Bright-field TEM image of the film with highlighted selected diffraction area (SA). (e) SAD with highlighted plane corresponding to the $BiVO_4$ phase shown in dark field TEM image (f). (g) Bright-field TEM image of the VO_2-phase in Bragg contrast and corresponding SAD (h).

present in the VO_2:Bi library as Bi > 0.29 at%. As shown in Fig. S3,† the resistivity of the VO_2:Bi library at lower temperatures, *e.g.*, 40 °C, didn't change too much. In comparison, at higher temperatures, *e.g.*, 100 °C, it increases more obviously. Although the second phase $BiVO_4$ has much higher resistivity ($\sim 10^8$ Ω cm), its presence didn't elevate the overall resistivity of the VO_2:Bi library, probably due to its low amount. Interestingly, the tendency of resistivity change of metallic VO_2:Bi thin film (at 100 °C) along the increasing Bi content is coincident with the change of T_c: after a slight decrease at 0.08 at%, it increases within the Bi content of 0.08–0.29 at%, until Bi > 0.29 at%, where only a slight change is observed.

In the thin film library, the Bi content is not the only parameter which could affect T_c. There might be also a variation in oxygen-to-vanadium ratio along the library, inherently stemming from the sputter geometry, *i.e.*, the V atomic wedge and a possible O-gradient, as the O_2 inlet is close to the V-rich side of the library (shown in Fig. 1). The resulting variation in stoichiometry of VO_2 can also influence T_c. For example, T_c tends to decrease with O-deficiency and increase in over-stoichiometric VO_2. Another parameter is film thickness, which affects the grain size growth and thus T_c. It has been reported that smaller grain size can lead to decreased T_c, because a higher density of grain boundaries results in more defects promoting the phase nucleation.[28]

To rule out the possibility that the increase of T_c originates from the fabrication method, a V–O reference library was fabricated under the same deposition condition as that of VO_2:Bi library without sputtering the Bi_2O_3 target. It is reasonable to assume that the thickness and oxygen variation originated from the deposition layout should be comparable for both libraries. The V–O library studied here was confirmed to be single VO_2 phase at all MAs by XRD measurements (not shown). The $R(T)$ curves of the V–O reference library were studied and T_c of the thin films along the V–O library was plotted in Fig. 8 in comparison with that of VO_2:Bi library.

It turns out that T_c of the V–O library decreases along the direction from V-rich side to Bi-rich side, contrary to the increasing tendency in the VO_2:Bi library, which confirms the role of Bi in increasing the T_c of VO_2. Moreover, a detailed XPS surface characterization (not shown) on the V–O library also indicated a higher V^{5+}/V^{4+} and slight decrease of V^{5+}/V^{4+} at the V-rich side, similar to what was observed in the VO_2:Bi library. It suggests that O-rich VO_2 forms at the V-rich side due to the sputter layout, which might account for the higher V^{5+}/V^{4+} ratio and slight decrease of T_c in the VO_2:Bi library at first two MAs. For the MAs with higher Bi until 0.29 at%, the influence of Bi doping becomes more profound, which leads to the increase of V^{5+}/V^{4+} and T_c. It is noteworthy that T_c of V-rich VO_2:Bi thin film is higher than reported value of ~68 °C for VO_2, which might be partly attributed to the stress of the film, as tensile stress could increase T_c.[29]

The dopant-induced influence of lattice distortion and charge doping on the phase transformation in doped VO_2 systems is still under debate. For instance, the role of lattice distortion is emphasized in some studies on $V_{1-x}W_xO_2$.[10,30] They found that the lattice distortion around W atoms promotes the formation of rutile-like VO_2 nuclei in monoclinic lattice, which propagates through the VO_2 M1 matrix and lower the thermal energy barrier for the phase transformation. In contrast, some[21,22] claim that the electron doping enhances the charge carriers in $V_{1-x}W_xO_2$, due to the extra two electrons from W-doping, which affects the band structure and facilitate the transformation to the metallic phase. Another study[11] suggests that both electronic distribution and local structure perturbation are responsible for the reduction of T_c in $V_{1-x}W_xO_2$. A comparative study[31] on W- and Ti-doped VO_2 concludes that the role of charge doping is more prominent in regulating T_c,

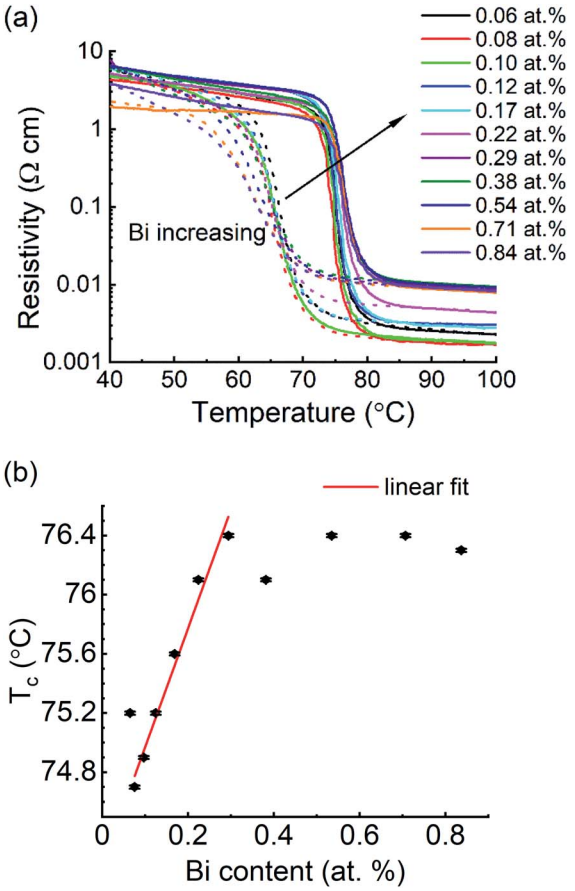

Fig. 7 Phase transformation properties of VO_2:Bi thin films in dependence of Bi content from 0.06 to 0.84 at%: (a) $\rho(T)$ curves, solid lines denote heating cycles and dotted lines cooling cycles, (b) T_c in dependence of Bi content, with a linear fit (red line) in the Bi range from 0.08 to 0.29 at%. The error of T_c is from the Gaussian fitting of the first derivative of $\rho(T)$, d log ρ/dT.

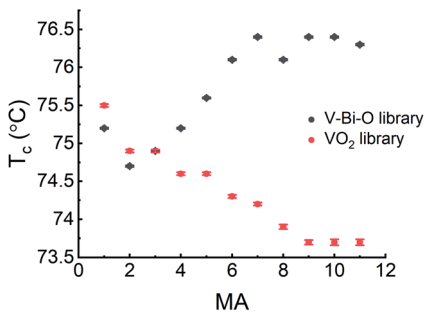

Fig. 8 T_c of V–O reference library and VO_2:Bi library at different MAs. The error of T_c is from the Gaussian fitting of the first derivative of $\rho(T)$, d log ρ/dT.

although the local structure perturbation induced by dopants is also present. In the current study, the large ionic size of Bi^{3+} seems not to give rise to significant structure distortion in VO_2 (M1) to reduce the T_c values. Instead, the large difference of ionic size between Bi^{3+} and V^{4+} limits the solubility of Bi^{3+} in VO_2 to ~0.29 at%. In the composition range of the VO_2:Bi library with soluble Bi^{3+}, the variations of V^{5+}/V^{4+} ratio and T_c show an almost similar trend with increasing Bi content, which suggests that the effect of charge doping on the phase transformation behavior is more prominent. When doping with Bi^{3+} holes are introduced into the VO_2:Bi system due to the charge compensation and are trapped as discrete V^{5+} ions at cation sites neighboring to the Bi^{3+}, which is in accordance with the increase of V^{5+}/V^{4+} ratio. The effect of elemental doping with higher or lower valence than V^{4+} on tuning the transition temperature is comparable with the non-stoichiometry of VO_2.[32,33] Here the Bi^{3+}-doped VO_2 behaves like over-stoichiometric VO_2 with excess O. As reported,[34] excess O gives rise to more V^{5+}, higher T_c and increasing metallic resistivity, which have all been observed in the current study. In addition, compared to V^{4+}, V^{5+} ions tend to stabilize the low-temperature structure, because the V^{5+} ion, with small size and empty d orbitals, is in favor of lower anion coordination and not stable in an oxygen octahedron of the high temperature structure.[35] As a result, the T_c values are increased with Bi doping. Similar correlations have been reported in previous studies on Al^{3+}-, Ga^{3+}- and most recently Ge-doped VO_2 systems.[35,36] By using Bi^{3+} as dopant, both the size and charge effects of the dopant on the MIT of VO_2 are evaluated. The higher ion size of Bi^{3+} does not cause obvious lattice distortions to reduce the T_c, which could otherwise support the mechanism of Peierls-transition in VO_2. In contrast, the charge doping plays a more prominent role in increasing T_c, which suggests that the Mott-transition is probably the main cause of the VO_2 MIT.

4. Conclusions

A VO_2:Bi library was fabricated by reactive co-sputtering, with Bi content ranging from 0.06 to 0.84 at%. Although only VO_2 M1 phase was detected by XRD, a detailed microstructure study revealed the presence of a second phase $BiVO_4$ for Bi > 0.29 at%, which suggests that the solubility of Bi^{3+} in VO_2 is limited to ~0.29 at%. The large ionic size of Bi^{3+} limits its solubility in VO_2, and no obvious lattice distortion was indicated in the X-ray diffraction patterns. Studies on the oxidation state of V by XPS indicates that adding Bi^{3+} into VO_2 generates more V^{5+}, meanwhile transformation properties studied by $\rho(T)$ curves of the VO_2:Bi library shows that T_c of VO_2:Bi increases from 74.7 to 76.4 °C by 8 K per at% Bi at Bi content range of 0.08–0.29 at%. The good agreement between increasing V^{5+}/V^{4+} and T_c suggests that in the VO_2:Bi library the effect of charge doping from Bi^{3+} on the phase transformation of VO_2 is more profound than the lattice distortion.

Conflicts of interest

There are no conflicts to declare.

Acknowledgements

The authors would like to thank ZGH for support in XRD, SEM, TEM measurements and FIB sample preparation. This work was supported by the German Research Foundation (DFG) (Project number LU 1175/18-1).

References

1 F. J. Morin, *Phys. Rev. Lett.*, 1959, **3**, 34.
2 Y. Zhao, J. Hwan Lee, Y. Zhu, M. Nazari, C. Chen, H. Wang, A. Bernussi, M. Holtz and Z. Fan, *J. Appl. Phys.*, 2012, **111**, 53533.
3 R. Shi, N. Shen, J. Wang, W. Wang, A. Amini, N. Wang and C. Cheng, *Appl. Phys. Rev.*, 2019, **6**, 11312.
4 S. Y. Li, G. A. Niklasson and C. G. Granqvist, *J. Appl. Phys.*, 2014, **115**, 53513.
5 F. Xu, X. Cao, H. Luo and P. Jin, *J. Mater. Chem. C*, 2018, **6**, 1903–1919.
6 D. Ruzmetov, G. Gopalakrishnan, C. Ko, V. Narayanamurti and S. Ramanathan, *J. Appl. Phys.*, 2010, **107**, 114516.
7 A. Rúa, F. E. Fernández and N. Sepúlveda, *J. Appl. Phys.*, 2010, **107**, 74506.
8 K. Liu, C. Cheng, Z. Cheng, K. Wang, R. Ramesh and J. Wu, *Nano Lett.*, 2012, **12**, 6302–6308.
9 X. Tan, T. Yao, R. Long, Z. Sun, Y. Feng, H. Cheng, X. Yuan, W. Zhang, Q. Liu, C. Wu, Y. Xie and S. Wei, *Sci. Rep.*, 2012, **2**, 466.
10 C. Si, W. Xu, H. Wang, J. Zhou, A. Ablat, L. Zhang, J. Cheng, Z. Pan, L. Fan, C. Zou and Z. Wu, *Phys. Chem. Chem. Phys.*, 2012, **14**, 15021–15028.
11 Y. Wu, L. Fan, W. Huang, S. Chen, S. Chen, F. Chen, C. Zou and Z. Wu, *Phys. Chem. Chem. Phys.*, 2014, **16**, 17705–17714.
12 D. Ruzmetov, S. D. Senanayake, V. Narayanamurti and S. Ramanathan, *Phys. Rev. B*, 2008, **77**, 1217.
13 O. Nájera, M. Civelli, V. Dobrosavljević and M. J. Rozenberg, *Phys. Rev. B*, 2017, **95**, 035113.
14 T. J. Huffman, C. Hendriks, E. J. Walter, J. Yoon, H. Ju, R. Smith, G. L. Carr, H. Krakauer and M. M. Qazilbash, *Phys. Rev. B*, 2017, **95**, 075125.
15 A. Cavalleri, T. Dekorsy, H. H. W. Chong, J. C. Kieffer and R. W. Schoenlein, *Phys. Rev. B: Condens. Matter Mater. Phys.*, 2004, **70**, 161102.
16 M. Soltani, M. Chaker, E. Haddad, R. V. Kruzelecky and J. Margot, *Appl. Phys. Lett.*, 2004, **85**, 1958–1960.
17 Y. Jiazhen, Z. Yue, H. Wanxia and T. Mingjin, *Thin Solid Films*, 2008, **516**, 8554–8558.
18 C. Piccirillo, R. Binions and I. P. Parkin, *Eur. J. Inorg. Chem.*, 2007, 4050–4055.
19 B. L. Brown, M. Lee, P. G. Clem, C. D. Nordquist, T. S. Jordan, S. L. Wolfley, D. Leonhardt, C. Edney and J. A. Custer, *J. Appl. Phys.*, 2013, **113**, 173704.
20 W. Bruckneb, U. Gerlach, H. P. Bruckner, W. Moldenhaueb and H. Opperman, *Phys. Status Solidi*, 1977, **42**, 295.
21 B. G. Chae and H. T. Kim, *Phys. B*, 2010, **405**, 663–667.
22 C. Tang, P. Georgopoulos, M. E. Fine, J. B. Cohen, M. Nygren, G. S. Knapp and A. Aldred, *Phys. Rev. B: Condens. Matter Mater. Phys.*, 1985, **31**, 1000.
23 N. Wang, M. Duchamp, R. E. Dunin-Borkowski, S. Liu, X. Zeng, X. Cao and Y. Long, *Langmuir*, 2016, **32**, 759–764.
24 X. Cao, N. Wang, S. Magdassi, D. Mandler and Y. Long, *Sci. Adv. Mater.*, 2014, **6**, 558–561.
25 X. Wang, L. Yan, Y. Li and Y. Cao, *J. Inorg. Mater.*, 2015, **30**, 1228.
26 M. Mayer, *AIP Conf. Proc.*, 1999, **475**, 541–544.
27 X. Wang, E. Suhr, L. Banko, S. Salomon and A. Ludwig, *ACS Appl. Electron. Mater.*, 2020, **2**, 1176–1183.
28 M. J. Miller and J. Wang, *J. Appl. Phys.*, 2015, **117**, 34307.
29 Y. Muraoka and Z. Hiroi, *Appl. Phys. Lett.*, 2002, **80**, 583–585.
30 J. M. Booth and P. S. Casey, *Phys. Rev. Lett.*, 2009, **103**, 86402.
31 Y. Wu, L. Fan, Q. Liu, S. Chen, W. Huang, F. Chen, G. Liao, C. Zou and Z. Wu, *Sci. Rep.*, 2015, **5**, 9328.
32 S. Zhang, J. Y. Chou and L. J. Lauhon, *Nano Lett.*, 2009, **9**, 4527–4532.
33 E. Strelcov, A. Tselev, I. Ivanov, J. D. Budai, J. Zhang, J. Z. Tischler, I. Kravchenko, S. V. Kalinin and A. Kolmakov, *Nano Lett.*, 2012, **12**, 6198–6205.
34 E. Kusano and J. A. Theil, *J. Vac. Sci. Technol., A*, 1989, **7**, 1314–1317.
35 J. B. Goodenough, *J. Solid State Chem.*, 1971, **2**, 490–500.
36 A. Krammer, A. Magrez, W. A. Vitale, P. Mocny, P. Jeanneret, E. Guibert, H. J. Whitlow, A. M. Ionescu and A. Schüler, *J. Appl. Phys.*, 2017, **122**, 45304.